*Int. J. Therm. Sci.* (2001) 40, 1011–1020

S1290-0729(01)01286-8/FLA

# Numerical study of the evaporative cooling of liquid film in laminar mixed convection tube flows

M'barek Feddaoui, El Mustapha Belahmidi *, Ahmed Mir, Abdelaziz Bendou

*Groupe de Recherche sur l'Energie et la Thermique (GRETH), EST B.P. 33/s, Agadir, Morocco*

(Received 11 October 2000, accepted 6 February 2001)

**Abstract** — A numerical study is reported to investigate the evaporative cooling of liquid film falling along a vertical tube. A marching procedure is employed for solution of the equation of mass momentum, energy and concentration in the flow. Numerical results for air-water system are presented. The effects of flow conditions on the film cooling mechanism are discussed. Results show that a better liquid film cooling is noticed for a system having a higher inlet liquid temperature $T_{L0}$, a higher gas flow Reynolds number $Re$ or a lower liquid flow rate $\Gamma_0$. Additionally, the results indicate that the convection of heat by the flowing water film becomes the main mechanism for heat removal from the interface. © 2001 Éditions scientifiques et médicales Elsevier SAS

**heat and mass transfer / falling water film cooling / vertical tube / evaporation / mixed convection**

## Nomenclature

| | | |
|---|---|---|
| $c_p$ | specific heat | $J{\cdot}kg^{-1}{\cdot}K^{-1}$ |
| $c_{pa}$ | specific heat of air | $J{\cdot}kg^{-1}{\cdot}K^{-1}$ |
| $c_{pv}$ | specific heat of water vapour | $J{\cdot}kg^{-1}{\cdot}K^{-1}$ |
| $D$ | mass diffusivity | $m^2{\cdot}s^{-1}$ |
| $g$ | gravitational acceleration | $m{\cdot}s^{-2}$ |
| $h_M$ | masse transfer coefficient | $m{\cdot}s^{-1}$ |
| $h_T$ | heat transfer coefficient | $W{\cdot}m^{-2}{\cdot}K^{-1}$ |
| $\dot{m}_I$ | evaporating mass flux | $kg{\cdot}m^{-2}{\cdot}s^{-1}$ |
| $Mr$ | nondimentional accumulated mass evaporation rate | |
| $M_a$ | molar mass of air | $kg{\cdot}mol^{-1}{\cdot}K^{-1}$ |
| $M_v$ | molar mass of vapour | $kg{\cdot}mol^{-1}{\cdot}K^{-1}$ |
| $Nu_I$ | local Nusselt number of latent heat transport | |
| $Nu_s$ | local Nusselt number of sensible heat transport | |
| $Nu_x$ | overall Nusselt number | |
| $p$ | mixture pressure | Pa |
| $p_d$ | dynamic pressure | Pa |
| $Pr$ | Prandtl number | |
| $q_{sI}$ | sensible heat flux | $W{\cdot}m^{-2}$ |
| $q_{lI}$ | latent heat flux | $W{\cdot}m^{-2}$ |
| $q_I$ | total heat flux | $W{\cdot}m^{-2}$ |
| $r$ | co-ordinate in $r$-direction | m |
| $R$ | radius of the tube | m |
| $Re$ | Reynolds number of the gas stream | |
| $Re_L$ | liquid film Reynolds number | |
| $Sc$ | Schmidt number | |
| $Sh_x$ | interfacial Sherwood number | |
| $T$ | temperature | K |
| $T_{L0}$ | inlet liquid film temperature | K |
| $T_{Le}$ | exit liquid film temperature | K |
| $T_0$ | inlet temperature | K |
| $T_w$ | wall temperature | K |
| $u$ | axial velocity | $m{\cdot}s^{-1}$ |
| $v$ | radial velocity | $m{\cdot}s^{-1}$ |
| $w$ | mass fraction of vapour | |
| $x$ | dimensional axial co-ordinate | m |
| $X$ | dimensionless axial co-ordinate | |

*Greek symbols*

| | | |
|---|---|---|
| $\Gamma_0$ | inlet liquid mass flow rate | $kg{\cdot}m^{-1}{\cdot}s^{-1}$ |
| $\delta_x$ | local liquid film thickness | m |
| $\gamma$ | latent heat of vaporisation | $J{\cdot}kg^{-1}$ |
| $\lambda$ | thermal conductivity | $W{\cdot}m^{-1}{\cdot}K^{-1}$ |
| $\mu$ | dynamic viscosity | $kg{\cdot}m^{-1}{\cdot}s^{-1}$ |
| $\nu$ | kinematics viscosity | $m^2{\cdot}s^{-1}$ |

* Correspondence and reprints.
*E-mail addresses:* feddaoui@esta.ac.ma (M. Feddaoui), belahmidi@esta.ac.ma (E.M. Belahmidi), mir@esta.ac.ma (A. Mir), bendou@esta.ac.ma (A. Bendou).

| | | |
|---|---|---|
| $\rho$ | density . . . . . | kg·m$^{-3}$ |
| $\phi$ | relative humidity at inlet | |

*Subscripts*

| | |
|---|---|
| b | bulk quantity |
| I | condition at the gas-liquid interface |
| G | mixture (gas + vapour) |
| L | liquid film |
| 0 | condition at inlet |
| v | vapour |
| w | condition at wall |

## 1. INTRODUCTION

Gas-liquid flow systems with coupled heat and mass transfer is encountered in many industrial processes. Notable examples include cooling towers, condenser, evaporator, drying and a heat recovery process from waste heat water. Because of its practical importance, a long number of theoretical analyses have been made concerning the heat and mass transfer problems. The study of evaporative cooling of liquid film in laminar mixed convection tube flows has not been fully explored. The purpose of this article is to enhance our understanding of the evaporative cooling process by performing a detailed analysis for interfacial heat and mass transfer in air over a falling water film.

Computational studies of liquid film cooling have been carried out by a number of investigators. Examples include the work of liquid film cooling along a flat plate in a gas stream has been reported by Shembharkar and Pai [1], Yan and Soong [2–4] and Tsay et al. [5]. Laminar mixed convection heat and mass transfer in wetted vertical ducts has been analysed by Lin et al. [6], Tsay and Yan [7]. In their analyses, the liquid film on the wetted wall was assumed to be extremely thin so that it was regarded as a boundary condition for heat and mass transfer only. A similar study was conducted by Fedorov et al. [8] but with turbulent flow. The evaporative cooling of liquid film in natural convection channel flows was explored by Yan et al. [9, 10]. The results show that the cooling of the liquid film is mainly caused by the latent heat transfer associated with its evaporation. Recently Yan [11], published a study to investigate the effect of finite film evaporation on the mixed convection heat and mass transfer in a vertical pipe. He found that the assumption of an extremely thin film is seriously in error.

The detailed analysis, including transport processes in the gas flow and liquid film, was simultaneously performed for turbulent gas flow over a vaporising liquid film by Baumann and Thiel [12] and He et al. [13]. In these studies, the laminar Couette flow for the liquid film was used to simplify the problem. Yan [14] investigate the natural convection heat and mass transfer in a vertical pipe. He found that as the $Re_L$ increases, the Nusselt type approximation adopted by [12, 13] becomes more questionable. In addition, Yan [15] applied a low Reynolds number $k$–$\varepsilon$ turbulent model in the gas flow region to predict the turbulent mixed convection heat transfer and fluid flow in vertical channel.

## 2. ANALYSIS

### 2.1. Physical model and assumption

The geometry of the problem under consideration is a vertical tube with cocurrent downstream flow of both the gas stream and the falling liquid film (*figure 1*). The thin liquid film is fed with an inlet liquid temperature $T_{L0}$, and inlet liquid mass flow rate $\Gamma_0$. The tube wall is thermally insulated. The flow enters the tube at temperature $T_0$, and at constant velocity $u_0$. An attempt has therefore, been made here to model the process with the following simplifying assumptions:

(1) The thermodynamic and thermophysical properties of air, water, and air–water vapour mixture are

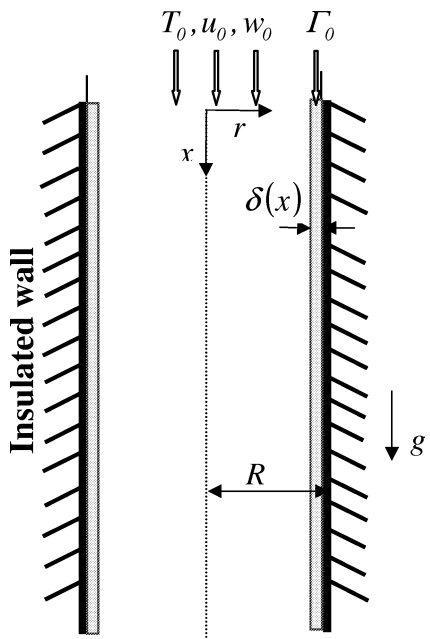


**Figure 1.** Schematic diagram of the physical system.

function of both local temperature and concentration. The thermophysical properties are available in Fujii et al. [16].

(2) Radiation heat transfer, viscous dissipation and other secondary effects are negligible.

(3) The Reynolds number of the water film flow is assumed to be lower than the critical value of $Re_{Lc} = 1500$ for laminar conditions quoted by Ueda and Tanaka [17].

(4) The thermodynamic equilibrium is assumed at the gas-liquid interface.

(5) The inertial terms are neglected in the momentum equation of the liquid film as compared with the diffusional term. Moreover, for the thin liquid film the axial transfers of momentum and energy are smaller than those in the radial direction.

## 2.2. Model equations

With the above assumptions, the steady laminar momentum and heat transfer in the liquid film can be described in the cylindrical co-ordinates by the following equations:

– Momentum

$$\frac{1}{r}\frac{\partial}{\partial r}\left[r\mu_{\mathrm{L}}\frac{\partial u_{\mathrm{L}}}{\partial r}\right]+\rho_{\mathrm{L}}g=0 \tag{1}$$

– Energy

$$\rho_{\mathrm{L}}c_{\mathrm{pL}}u_{\mathrm{L}}\frac{\partial T_{\mathrm{L}}}{\partial x}=\frac{1}{r}\frac{\partial}{\partial r}\left[r\lambda_{\mathrm{L}}\frac{\partial T_{\mathrm{L}}}{\partial r}\right] \tag{2}$$

The two-dimensional boundary layer flow in the gas side is governed by the following conservation equations:

– Continuity

$$\frac{\partial}{\partial x}(r\rho_{\mathrm{G}}u_{\mathrm{G}})+\frac{\partial}{\partial r}(r\rho_{\mathrm{G}}v_{\mathrm{G}})=0 \tag{3}$$

– Momentum

$$\rho_{\mathrm{G}}\left(u_{\mathrm{G}}\frac{\partial u_{\mathrm{G}}}{\partial x}+v_{\mathrm{G}}\frac{\partial u_{\mathrm{G}}}{\partial r}\right) =-\frac{dp_{\mathrm{d}}}{dx}+\frac{1}{r}\frac{\partial}{\partial r}\left[r\mu_{\mathrm{G}}\frac{\partial u_{\mathrm{G}}}{\partial r}\right]-(\rho_0-\rho_{\mathrm{G}})g \tag{4}$$

– Energy

$$\rho_{\mathrm{G}}c_{\mathrm{pG}}\left(u_{\mathrm{G}}\frac{\partial T_{\mathrm{G}}}{\partial x}+v_{\mathrm{G}}\frac{\partial T_{\mathrm{G}}}{\partial r}\right) =\frac{1}{r}\frac{\partial}{\partial r}\left[r\lambda_{\mathrm{G}}\frac{\partial T_{\mathrm{G}}}{\partial r}\right]+\rho_{\mathrm{G}}D(c_{\mathrm{pv}}-c_{\mathrm{pa}})\frac{\partial T_{\mathrm{G}}}{\partial r}\frac{\partial w}{\partial r} \tag{5}$$

– Species concentration

$$\rho_{\mathrm{G}}\left(u_{\mathrm{G}}\frac{\partial w}{\partial x}+v_{\mathrm{G}}\frac{\partial w}{\partial r}\right)=\frac{1}{r}\frac{\partial}{\partial r}\left[r\rho_{\mathrm{G}}D\frac{\partial w}{\partial r}\right] \tag{6}$$

## 2.3. Boundary and interfacial matching conditions

The boundary conditions are:

$$x=0: \quad u_{\mathrm{G}}=u_0, \quad T_{\mathrm{G}}=T_0, \quad w=w_0 \tag{7}$$

$$r=0: \quad \frac{\partial u_{\mathrm{G}}}{\partial r}=0, \quad \frac{\partial T_{\mathrm{G}}}{\partial r}=0, \quad \frac{\partial w}{\partial r}=0 \tag{8}$$

$$r=R: \quad u_{\mathrm{L}}=0, \quad \lambda_{\mathrm{L}}\frac{\partial T_{\mathrm{L}}}{\partial r}=0 \tag{9}$$

The solution from the liquid side and gas side satisfy the following interfacial matching conditions ($r = R - \delta$):

(a) Continuities of velocity and temperature

$$u_{\mathrm{I}}(x)=u_{\mathrm{G,I}}=u_{\mathrm{L,I}}, \qquad T_{\mathrm{I}}(x)=T_{\mathrm{G,I}}=T_{\mathrm{L,I}} \tag{10}$$

(b) Continuity of shear stress

$$\tau_{\mathrm{I}}=\left[\mu\frac{\partial u}{\partial r}\right]_{\mathrm{L,I}}=\left[\mu\frac{\partial u}{\partial r}\right]_{\mathrm{G,I}} \tag{11}$$

(c) The radial velocity component is non-zero due to the generation of vapour at the interface. Assuming that the gas-liquid interface is semi-permeable (that is, the solubility of air into the water is negligibly small, so that the air does not move radially to the interface), the velocity of the air–vapour mixture can be calculated by:

$$v_{\mathrm{I}}=-\frac{D}{(1-w_{\mathrm{I}})}\frac{\partial w}{\partial r} \tag{12}$$

The mass fraction at the interface $w_{\mathrm{I}}$ can be calculated using:

$$w_{\mathrm{I}}=\frac{M_{\mathrm{v}}P_{\mathrm{v},i}}{M_{\mathrm{a}}(P-P_{\mathrm{v},i})+M_{\mathrm{v}}P_{\mathrm{v},i}} \tag{13}$$

Where $P$ and $P_{\mathrm{v},i}$ are the total pressure and the vapour pressure at the interface, respectively. $M_{\mathrm{a}}$ and $M_{\mathrm{v}}$ are the molecular weights of air and vapour.

(d) Mass balance at the interface implying

$$\dot{m}_{\mathrm{I}}=\frac{\rho_{\mathrm{G}}D}{(1-w_{\mathrm{I}})}\frac{\partial w}{\partial r} \tag{14}$$

(e) Heat balance at the interface implying

$$\left[\lambda\frac{\partial T}{\partial r}\right]_{\mathrm{L,I}}=\left[\lambda\frac{\partial T}{\partial r}\right]_{\mathrm{G,I}}+\dot{m}_{\mathrm{I}}\cdot\gamma \tag{15}$$

Where $\gamma$ is the enthalpy of evaporation and $\dot{m}_I$, the vapour generation rate ($= -\rho_G v_I$).

The local heat exchange between the air stream and water film depends on two related factors: the interfacial temperature gradient on the air side results in sensible convective heat transfer, and the evaporative mass transfer rate on the water film side results in latent heat transfer. The total convective heat transfer from the film interface to the air stream can be expressed as follows:

$$q_I = q_{sI} + q_{lI} = \left[\lambda \frac{\partial T}{\partial r}\right]_{G,I} + \dot{m}_I \cdot \gamma \qquad (16)$$

The local Nusselt number along the interface gas-liquid, defined as:

$$Nu_x = \frac{h_T(2R)}{\lambda_G} = \frac{q_I(2R)}{\lambda_G(T_I - T_b)} \qquad (17)$$

Can be written as:

$$Nu_x = Nu_s + Nu_L \qquad (18)$$

Where $Nu_s$ and $Nu_L$ are the local Nusselt numbers for sensible and latent heat transfer, respectively, and are expressed as follows:

$$Nu_s = \frac{q_{sI}(2R)}{\lambda_G(T_I - T_b)} \qquad (19)$$

$$Nu_L = \frac{q_{lI}(2R)}{\lambda_G(T_I - T_b)} \qquad (20)$$

Basing the local mass-transfer coefficient on the diffusive mass flux, the local Sherwood number is defined as:

$$Sh_x = \frac{h_M(2R)}{D} = \frac{\dot{m}_I(1 - w_I)(2R)}{\rho_G D(w_I - w_b)} \qquad (21)$$

At every axial location, the overall mass balance in the gas flow and liquid film should be satisfied:

$$\frac{(R - \delta_0)^2}{2}\rho_G u_0 = \int_0^{R-\delta} r\rho_G u_G \,\mathrm{d}r + \int_0^x \rho_G v_I \,\mathrm{d}x \qquad (22)$$

$$\Gamma_0 = \int_{R-\delta}^{R} (r\rho u \,\mathrm{d}r)_L - \int_0^x \rho_G v_I \,\mathrm{d}x \qquad (23)$$

To improve the understanding of heat and mass transfer process, a nondimensional accumulated mass evaporation rate is introduced:

$$Mr = \frac{\int_0^x \dot{m}_I \,\mathrm{d}x}{\Gamma_0} = -\frac{\int_0^x \rho_G v_I \,\mathrm{d}x}{\Gamma_0} \qquad (24)$$

## 3. NUMERICAL METHOD

In view of the impossibility of obtaining an analytic solution for the non-linear coupling differential equations, the conjugated problem defined by the parabolic systems, equations (1)–(6) with the appropriate boundary conditions are solved by a finite difference numerical scheme. The axial convection terms are approximated by the backward difference and the radial convection and diffusion terms are approximated by the central difference. In the centreline ($r = 0$) of the tube the diffusional terms are singular. A correct representation can be found from an application of L'Hospital's rule. Each system of the finite-difference equations forms a tridiagonal matrix equation, which can be solved by the Thomas algorithm (Patankar [18]).

After specifying the flow and thermal conditions, the numerical solution is advanced forward and step by step as follows:

(1) For any axial location $x$, guesses $\frac{\mathrm{d}p_d}{\mathrm{d}x}$ and $\delta_x$.
(2) Solve the finite-difference forms of equations (1)–(6) simultaneously for $u$, $T$ and $w$.
(3) Numerically integrate (3) to find $v_G$.
(4) Check the mass conservation of both liquid film and gas flow by examining the satisfaction of the equations (22) and (23). If not, adjust $\frac{\mathrm{d}p_d}{\mathrm{d}x}$ and $\delta_x$ and repeat procedures 2 to 4.
(5) Check the satisfaction of the convergence of velocity, temperature and mass fraction. If the relative error between two consecutive iterations is small enough, i.e.:

$$\frac{\max|\psi_{i,j}^n - \psi_{i,j}^{n-1}|}{\max|\psi_{i,j}^n|} < 10^{-4} \qquad (25)$$

where $\psi$ represents the variables $u$, $T$ and $w$. If not, repeat procedures 1 to 5.

The correction of the pressure gradient and axial velocity profile at each axial station in order to satisfy the global mass flow constraint is achieved using a method due to Raithby and Schneider [19], described by Anderson et al. [20].

To obtain enhanced accuracy in the numerical computations, grids are chosen to be non-uniform in both axial and radial directions. Accordingly the grids are compressed towards the interface gas-liquid and towards the entrance of tube. Grid-independence of the results by employing several arrangements of grid point in $x$ and $r$ directions is tested and the corresponding results are presented in *table I*. It is found from *table I* that the differences in the local Nusselt number from computations

TABLE I
Comparisons of local interfacial Nusselt number $Nu_x$ for various grid arrangements for $\Gamma_0 = 0.01$ kg·m$^{-1}$·s$^{-1}$, $T_{L0} = 40\,^{\circ}$C, $Re = 2 \times 10^3$.

| | $I \times J \times K$ | | | | |
|---|---|---|---|---|---|
| $X$ | $201 \times 121 \times 61$ | $101 \times 121 \times 61$ | $101 \times 61 \times 31$ | $51 \times 61 \times 31$ | $51 \times 31 \times 21$ |
| 6.15 | 42.46 | 43.84 | 43.88 | 46.60 | 46.29 |
| 17.36 | 25.74 | 25.94 | 25.97 | 26.62 | 26.85 |
| 45.86 | 20.05 | 20.13 | 20.15 | 20.31 | 20.47 |
| 71.41 | 19.76 | 19.80 | 19.82 | 19.92 | 20.06 |
| 100.00 | 20.23 | 20.26 | 20.27 | 20.33 | 20.47 |

I: total grid points in the axial direction; J: total grid points in the radial direction at the gas side;
K: total grid points in the radial direction at the liquid side.

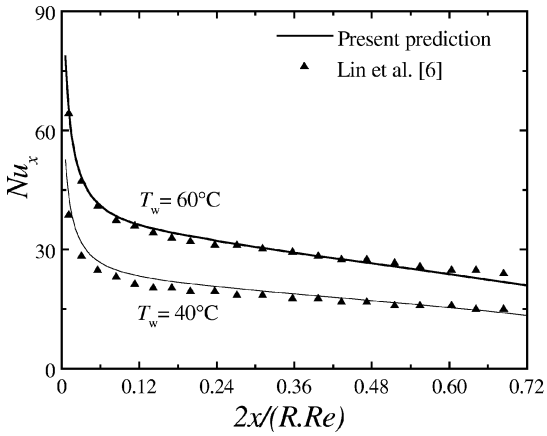


**Figure 2.** Local Nusselt number $Nu_x$ along the tube for $Re = 2000$, $T_0 = 20\,^{\circ}$C.

using grids ranging from $51 \times 31 \times 21$ to $201 \times 121 \times 61$ were always within 4 percent. To reduce the cost of computation, the $101 \times 61 \times 31$ grid was chosen for the rest of study.

In *figure 2* the present predictions of local Nusselt number $Nu_x$ are compared with the prediction of Lin et al. [6] in the case of vaporising an extremely thin liquid film on the tube wall in laminar mixed convection flows. Excellent agreement between the present predictions and those of Lin et al. [6]. In view of these validations, the present numerical algorithm and employed grid layout are adequate to obtain accurate results for practical purpose.

## 4. RESULTS AND DISCUSSION

In order to examine the effects of flow conditions on the film cooling mechanism on mixed convection heat and mass transfer in a vertical tube, results are particularly presented for water film evaporation. The following set conditions are selected in the computation: the relative humidity of the ambient air is assigned as 50% at $T_0 = 20\,^{\circ}$C and 1 atm along a vertical tube with a radius $R = 0.03$ m.The inlet liquid temperature $T_{L0}$ is 40 or 60 °C, the liquid flow rate $\Gamma_0$ is chosen to be 0.001, 0.005 or 0.01 kg·m$^{-1}$·s$^{-1}$, and the inlet gas stream Reynolds number *Re* is 1000 or 2000.

Detailed heat transfer characteristics in the flow can be illustrated by examining the axial developments of the temperature profile in *figure 3 (a)* and *(b)* for the cases with $T_{L0} = 40\,^{\circ}$C and 60 °C at $\Gamma_0 = 0.01$ kg·m$^{-1}$·s$^{-1}$. The inset plots in the figure give the temperature profiles near the interface. According to the results in *figure 3*, at a given axial location the temperature in gas flow and liquid film increases monotonically with $r$. This implies that the directions of sensible heat transfer are from the interface toward the gas stream and from the wall to the interface. It is clearly seen in the inserted plots that the interfacial temperature decrease along the tube, also at a given axial location the temperature in the liquid film is relatively uniform because the film is rather thin.

The mass fraction distributions of the water vapour in the gas stream given in *figure 4* show that the mass fraction of water vapour in the gas flow in the central portion of the tube increase gradually as the air moves downstream. Also found that a larger amount of water vapour entering the air stream is for the case with higher $T_{L0}$. Due to the evaporative cooling, the interfacial temperature decreases along the tube. Therefore, the corresponding mass fraction of water vapour decreases with $X$ near the gas-liquid interface. These results are clearly illustrated in *figures 5–7*.

*Figure 5* shows the effects of various parameters on the axial distributions of the wall and interfacial

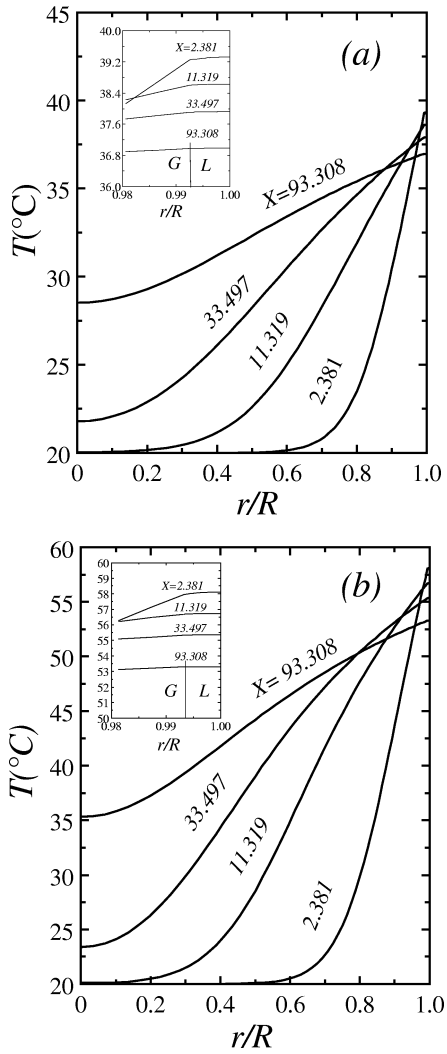


**Figure 3.** Distributions of axial temperature profiles for $Re = 2000$: (a) $\Gamma_0 = 0.01$ kg·m$^{-1}$·s$^{-1}$, $T_{L0} = 40\,^{\circ}$C; (b) $\Gamma_0 = 0.01$ kg·m$^{-1}$·s$^{-1}$, $T_{L0} = 60\,^{\circ}$C.

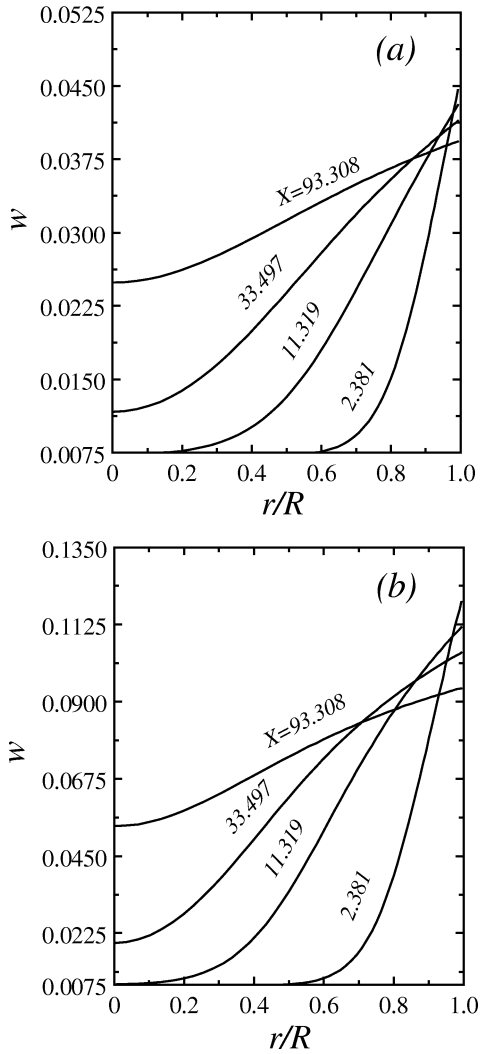


**Figure 4.** Distributions of axial mass fraction profiles for $Re = 2000$: (a) $\Gamma_0 = 0.01$ kg·m$^{-1}$·s$^{-1}$, $T_{L0} = 40\,^{\circ}$C; (b) $\Gamma_0 = 0.01$ kg·m$^{-1}$·s$^{-1}$, $T_{L0} = 60\,^{\circ}$C.

temperatures. The results indicate that the $T_I$ and $T_w$ decrease monotonically in the flow direction due to the evaporative cooling. This indicates that energy needed to sustain the evaporation must come from the internal energy of the liquid film. This is a consequence of a reduction in liquid film temperature. Therefore, the curves of $T_I$ and $T_w$ almost coincide with each other, except for the results near the inlet at higher liquid flow rate $\Gamma_0$.

As expected, the effectiveness of cooling liquid film is relatively poor for systems with larger liquid flow rate $\Gamma_0$. This is apparently due to the total internal energy stored in the liquid film is in larger quantity for the system with a larger liquid flow rate. Additionally, a larger temperature decrease results for a higher $T_{L0}$ as shown in *figure 5 (a)* and *(b)*. By comparing *figure 5 (a)* and *(c)*, it is found that a larger temperature drop is noted for a system with higher *Re*. Plotted in *figure 6* are the axial distributions of the interfacial mass fraction of water vapour along the gas-liquid interface. It is interesting to observe that both $T_I$ and $w_I$ develop in very similar fashion. As shown in *figure 5* the interfacial temperature decreases with $X$. Therefore, the corresponding mass fraction of water vapour decreases along the tube. *Figure 7* shows the total temperature drop of the liquid film as it flows from the inlet to the outlet for different conditions. It is

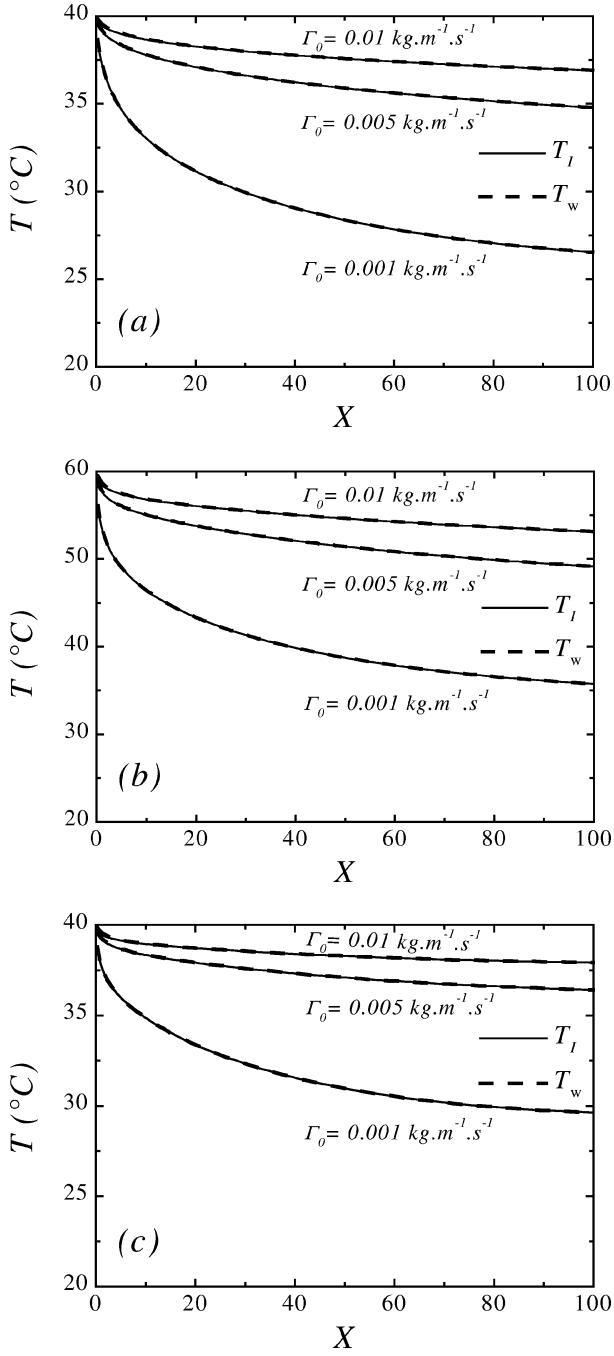


**Figure 5.** Distributions of interfacial and wall temperatures along the tube: (a) $Re = 2000$, $T_{L0} = 40\,°C$; (b) $Re = 2000$, $T_{L0} = 60\,°C$; (c) $Re = 1000$, $T_{L0} = 40\,°C$.

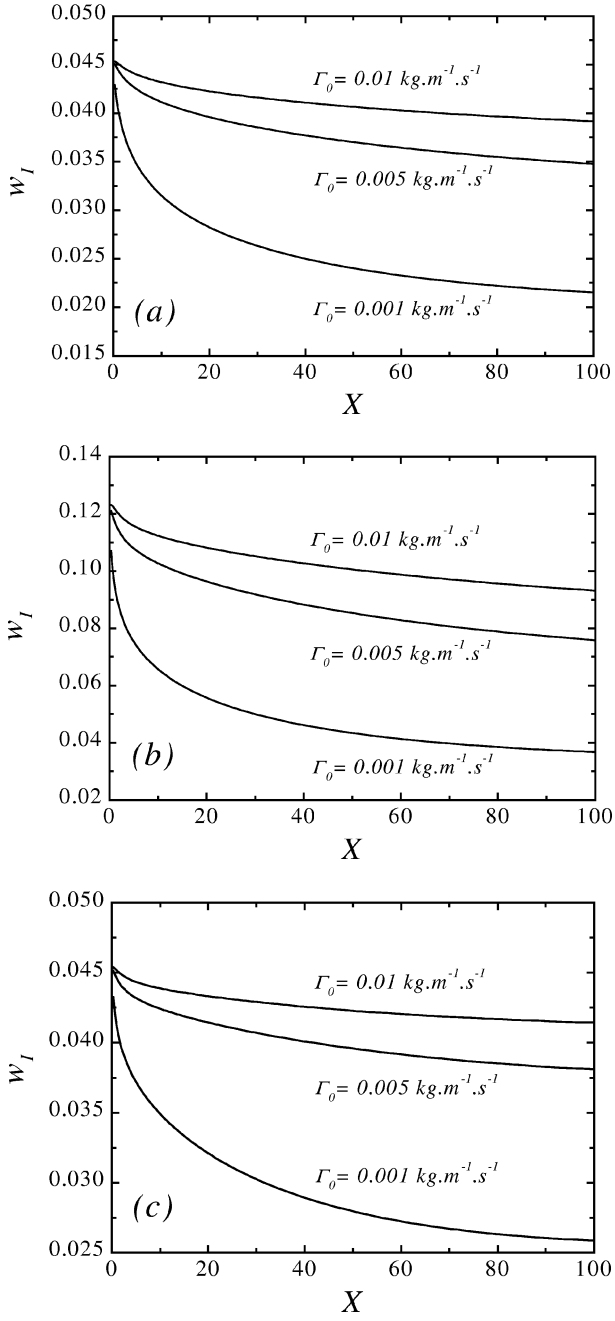


**Figure 6.** Distributions of mass fraction at the gas-liquid interface along the tube: (a) $Re = 2000$, $T_{L0} = 40\,°C$; (b) $Re = 2000$, $T_{L0} = 60\,°C$; (c) $Re = 1000$, $T_{L0} = 40\,°C$.

apparent in this plot that the larger liquid temperature drop is observed for a system with a higher $T_{L0}$ or lower $\Gamma_0$. This is due to the effective evaporative cooling in these cases.

To study the relative contributions of heat transfer through the sensible and latent heat flux, both the interfacial sensible Nusselt number $Nu_s$ and latent heat Nusselt number $Nu_L$ are demonstrated in *figure 8 (a)* and *(b)*. A smaller $Nu_s$ is found for a higher $T_{L0}$, and

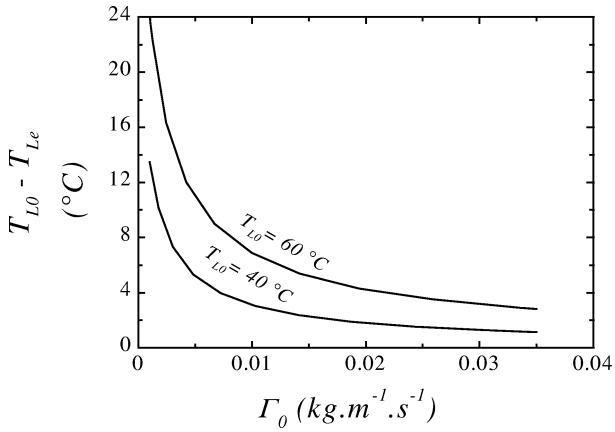


**Figure 7.** Effects of liquid mass flow rate on the temperature drops for $Re = 2000$.

for a larger liquid flow rate $\Gamma_0$. The system with a larger liquid flow rate $\Gamma_0$ or higher inlet water temperature $T_{L0}$ shows higher values of $Nu_L$. This is brought about by the larger latent heat transport in connection with the greater liquid film evaporation for higher $T_{L0}$ or larger $\Gamma_0$. By comparing the ordinate scales of *figure 8 (a)* and *(b)* indicates that the magnitude of $Nu_L$ is much larger than that of $Nu_s$, implying that the heat transfer resulting from latent heat exchange is much more effective. In *figure 8(c)* the total Nusselt number $Nu_x (Nu_s + Nu_L)$ is presented. It is clear that the system with a higher $T_{L0}$ or larger $\Gamma_0$ shows a large $Nu_x$.This implies that a better heat transfer is observed for a system with a larger $\Gamma_0$, and therefore the interfacial liquid film temperature is increased.

The variations of local Sherwood number $Sh_x$ are presented in *figure 9*. A larger Sherwood number results for systems with a lower inlet liquid temperature $T_{L0}$ or a smaller liquid flow rate $\Gamma_0$, due to the smaller evaporating (blowing) effect or opposing buoyancy effect. *Figure 10* shows the effects of $T_{L0}$ and *Re* on the distributions of *Mr*. The large liquid vaporisation is observed for a system with a higher inlet liquid temperature, which is clearly seen from *figure 5*. Also found in this plot that larger dimensionless accumulated evaporation rate is observed for the system with higher Reynolds number or smaller liquid flow rate by comparing *figure 10 (a)* and *(b)*. It also mentioning that a reduction in the film flow rate cause a greater film evaporation and *Mr* increase with *X* as the flow goes downstream.

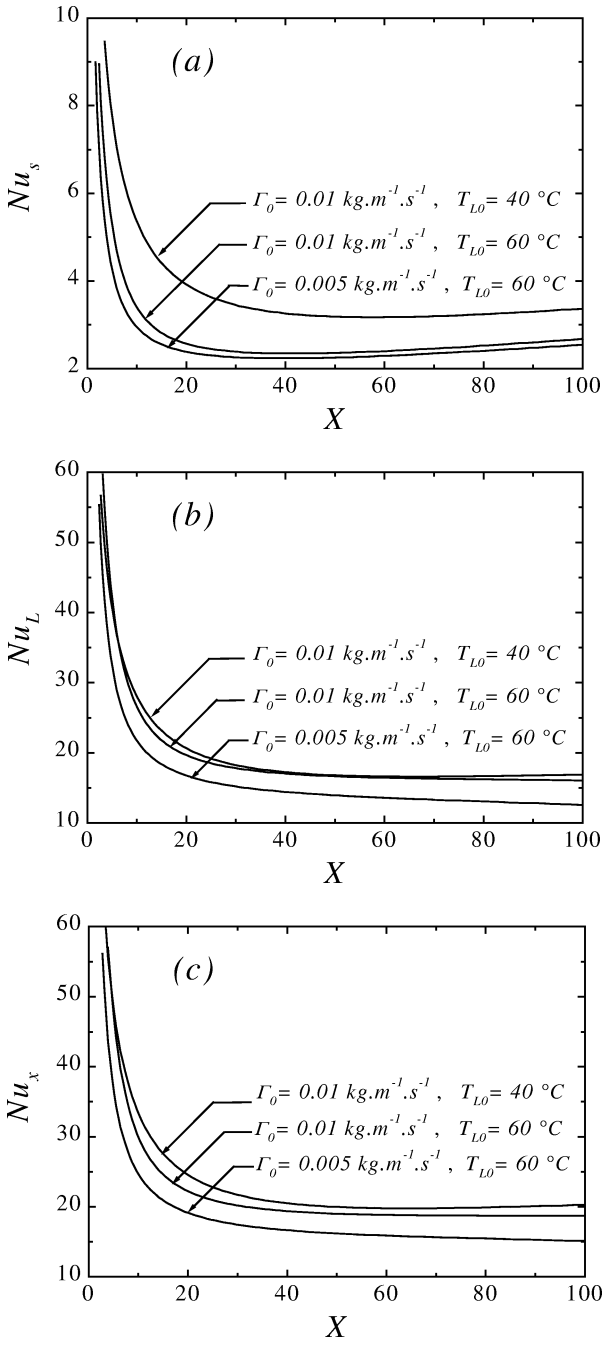


**Figure 8.** Distributions of local $Nu_s$, $Nu_L$, $Nu_x$ along the tube for $Re = 2000$.

## 5. CONCLUSION

The liquid film cooling along a vertical tube by solving the respective governing equations for the liquid film and the gas stream coupled through the interfacial matching conditions has been numerically studied. Based on the numerical results obtained, the following conclusion can be drawn:

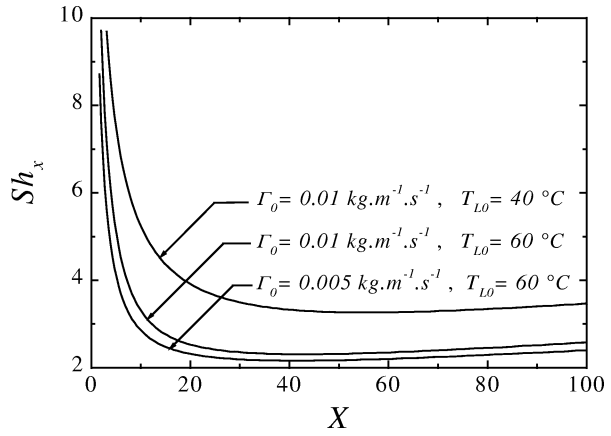


**Figure 9.** Distributions of local Sherwood number $Sh_x$ along the tube for $Re = 2000$.

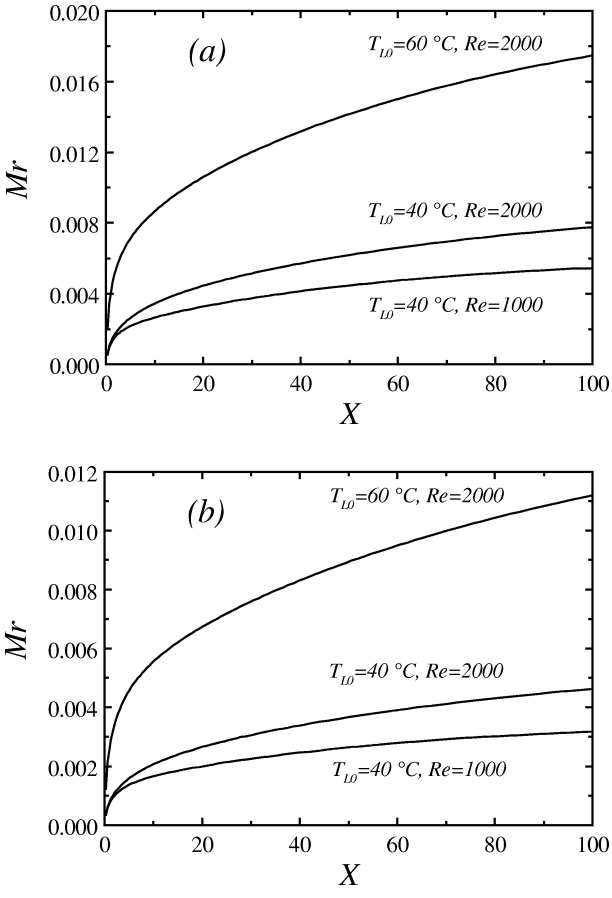


**Figure 10.** Distributions of dimensionless accumulated evaporation rate $Mr$ along the tube: (a) $\Gamma_0 = 0.005$ kg·m$^{-1}$·s$^{-1}$; (b) $\Gamma_0 = 0.01$ kg·m$^{-1}$·s$^{-1}$.

(1) The interfacial temperature and water vapour concentration decreases with the decreasing (increasing) liquid flow rate $\Gamma_0$ (Reynolds number $Re$).

(2) The larger liquid temperature drop is observed for systems with a higher inlet liquid temperature $T_{L0}$ or a lower liquid flow rate $\Gamma_0$.

(3) A larger sensible Nusselt number $Nu_s$ or Sherwood number $Sh_x$ results for system having a higher $\Gamma_0$ or $T_{L0}$.

(4) A rise in liquid flow rate $\Gamma_0$ or a reduction in $T_{L0}$ causes a large latent heat Nusselt number $Nu_L$.

(5) The convection of heat by the flowing liquid film becomes the main mechanism for heat removal from the interface.

It is recognised herein that the results presented above are based on a number of assumptions made in this study. In addition, it is also noted that the flowing gas in the vertical tube becomes turbulent for $Re > 2300$. For that, it may be worthwhile studying the effects of flow conditions on turbulent mixed convection heat and mass transfer. This will be carried out in near future.

## REFERENCES

[1] Shembharkar T.R., Pai B.R., Prediction of film cooling with a liquid coolant, Internat. J. Heat Mass Tran. 29 (1986) 899–908.

[2] Yan W.M., Soong C.Y., Numerical study of liquid film cooling along an inclined plate, Wärm und Stoffübertragung 28 (1993) 233–241.

[3] Yan W.M., Soong C.Y., Numerical study of liquid film cooling in a turbulent gas stream, Internat. J. Heat Mass Tran. 36 (1993) 3877–3885.

[4] Yan W.M., Soong C.Y., Convective heat and mass transfer along an inclined heated plate with film evaporation, Internat. J. Heat Mass Tran. 38 (1995) 1261–1269.

[5] Tsay Y.L., Lin T.F., Yan W.M., Cooling of falling liquid film through interfacial heat and mass transfer, Internat. J. Multiphase Flow 16 (1990) 853–865.

[6] Lin T.F., Chang C.J., Yan W.M., Analysis of combined buoyancy effects of thermal and mass diffusion on laminar forced convection heat transfer in a vertical tube, J. Heat Tran. 110 (1988) 337–344.

[7] Tsay H.C., Yan W.M., Binary diffusion and heat transfer in laminar mixed convection channel flows with uniform wall heat flux: extremely thin film thickness, Wärm und Stoffübertragung 26 (1990) 23–31.

[8] Fedorov A.G., Viskanta R., Mohamad A.A., Turbulent heat and mass transfer in asymmetrically heated, vertical parallel-plate channel, Internat. J. Heat Fluid Flow 18 (1997) 307–315.

[9] Yan W.M., Lin T.F., Tsay Y.L., Evaporative cooling of liquid film in through interfacial heat and mass transfer in a vertical channel: I—Experimental study, Internat. J. Heat Mass Tran. 34 (1991) 1105–1111.

[10] Yan W.M., Lin T.F., Evaporative cooling of liquid film in through interfacial heat and mass transfer in a

vertical channel: II—Numerical study, Internat. J. Heat Mass Tran. 34 (1991) 1113–1124.

[11] Yan W.M., Binary diffusion and heat transfer in mixed convection pipe flows with film evaporation, Internat. J. Heat Mass Tran. 36 (1993) 2115–2123.

[12] Baumann W.W., Thiele F., Heat and mass transfer in evaporating two-component liquid film flow, Internat. J. Heat Mass Tran. 33 (1990) 367–273.

[13] He S., An P., Li J., Jackson J.D., Combined heat and mass transfer in uniformly heated vertical tube with water film cooling, Internat. J. Heat Fluid Flow 19 (1998) 401–417.

[14] Yan W.M., The effect of liquid film vaporisation on natural convection heat and mass transfer in vertical tube, Canad. J. Chem. Engrg. 70 (1992) 452–462.

[15] Yan W.M., Evaporative cooling of liquid film in turbulent mixed convection channel flows, Internat. J. Heat Mass Tran. 41 (1998) 3719–3729.

[16] Fujii T., Kato Y., Mihara K., Expressions of transport and thermodynamic properties of air, stream and water, Report No. 66 (1977) 81–95.

[17] Ueda T., Tanaka H., Measurement of velocity, temperature and velocity fluctuation distributions in liquid films, Internat. J. Multiphase Flow 2 (1975) 261–272.

[18] Patankar S.V., Numerical Heat Transfer and Fluid Flow, Hemisphere/McGraw-Hill, New York, 1980, Chapter 6.

[19] Raithby G.D., Schneider G.E., Numerical solutions of problems in incompressible fluid flow: treatment of the velocity-pressure coupling, Numer. Heat Tran. 2 (1979) 417–440.

[20] Anderson D.A., Tannehill J.C., Pletcher R.H., Computational Fluid Mechanics and Heat Transfer, Hemisphere/McGraw-Hill, New York, 1984.